3

Photolithography and Self-Aligned Subtractive and Additive Patterning of Conductive Materials

Gert Homm, Steve Petznick, Torsten Henning and Peter J. Klar
Justus Liebig University,
Institute of Experimental Physics I, Gießen
Germany

1. Introduction

Quantum theory predicts a number of phenomena for materials scaled down to a size where confinement effects occur in one or more dimensions. Numerous devices that are based on these effects have been developed, as for example tunnel diodes, quantum well lasers, etc. An essential component in many of these device concepts are interfaces between conductive materials. To make the devices as efficient as possible in a reproducible way, the interfaces need to be controllable and tunable in their shape, morphology, and transport properties. For multilayer growth, investigations have already shown that a proper control of the quality of the interfaces between the stacked layers is of major importance for the device performance (Fasol et al., 1988; Hillmer et al., 1990). For in-plane interfaces, however, a proper characterization is still missing. To date and to our knowledge, only investigations of grain boundaries have been reported, in which the interfaces were arranged randomly (Schwartz, 1998; Watanabe, 1985; 1993; Watanabe & Tsurekawa, 1999).

A typical example are thermoelectric materials. Theory predicts that the thermoelectric figure of merit of a material

$$ZT = \frac{S^2\sigma}{\kappa}T, \tag{1}$$

where S is the Seebeck coefficient, σ the electrical conductivity and κ the thermal conductivity, could be significantly improved by reducing the dimensions of this material, namely by artificial structuring (Dresselhaus et al., 2007; Hicks & Dresselhaus, 1993a;b). As can be seen from equation (1), an improvement can be achieved by either increasing $S^2\sigma$ (the so called power factor) or by decreasing κ, without affecting the other parameters in an unwanted way. Assuming a constant Seebeck coefficient, the equation (1) implies that materials with a high electrical conductivity and a low thermal conductivity are desired, a design goal which, for metals, is somewhat contradicted by the Wiedemann-Franz law (Franz & Wiedemann, 1853; Lorenz, 1872). This directly leads to semiconductors as the materials class of choice for thermoelectrics. Here, numerous advantages over the metals can be used: The free carrier concentration can be adjusted by doping such that the electric conductivity is still fairly high, but the thermal conductivity is dominated by phonon transport. Simultaneously, the thermal conductivity can be reduced further by phonon blocking almost without affecting the free carrier transport, an approach for which various methods have been developed.

One fairly simple and effective way of improving the thermoelectric figure of merit is to take a thermoelectric material, e.g. PbTe, and then try to enhance it by ball milling and subsequent compacting. This method turned out to further improve the thermoelectric figure of merit of the bulk material due to a lowering of the thermal conductivity, while the electrical conductivity and the Seebeck coefficient remained high (Sootsman et al., 2009). This procedure has been applied to ZnO as well, with similar results, namely the reduction of the thermal conductivity by growing a highly disordered polycristalline material, i. e., by introducing interfaces (Alvarez-Quintana et al., 2010; Huang et al., 2011; Igamberdiev et al., 2010). A more defined way of introducing interfaces is to grow multilayers. The thermoelectric properties are then measured in cross-plane direction, i. e. perpendicular to the sample surface. High figures of merit could be achieved this way (Venkatasubramanian, 2000; Venkatasubramanian et al., 2001), but the sample preparation is comparatively complex, and for some applications, an in-plane geometry is more desirable. An elegant way to introduce well defined interfaces in-plane with a relatively simple process is the lateral structuring of thin films with alternating materials. Calculations show that for materials with incompatible phonon dispersion relations, the propagation of phonons of certain energies across the interfaces is suppressed (Bachmann et al., 2011; Bies et al., 2000; Capinski et al., 1999; Chen, 1998; Daly et al., 2003; Müller et al., 1994; Yang & Chen, 2003; Yao, 1987).

Motivated by this prediction we developed the sample preparation process that uses photolithography and self-aligned pattern transfer for defining lateral interfaces in thin-film structures and that will be detailed in the following. In fig. 1, a lateral structure with interfaces between undoped ZnO and Al-doped ZnO is shown as the typical result of this process. A

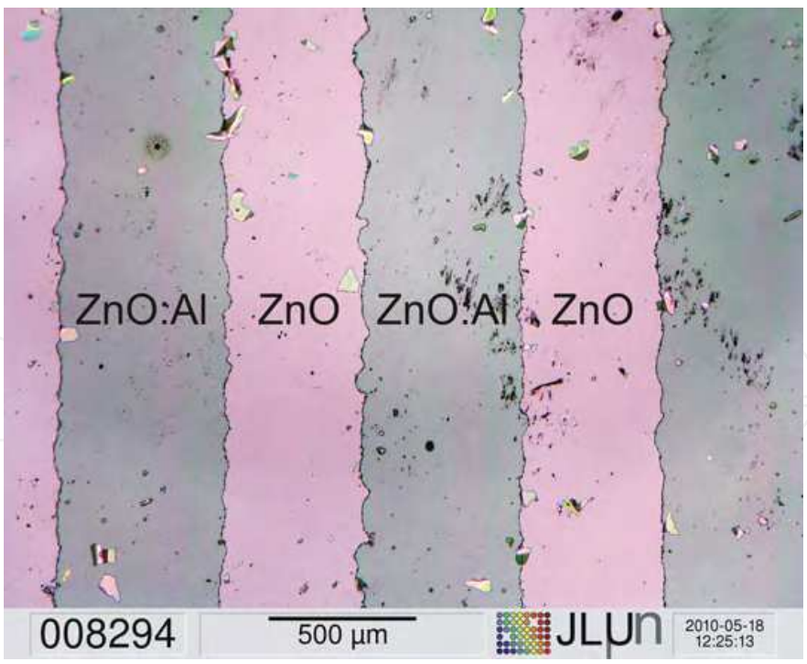

Fig. 1. Optical micrograph of structured alternating ZnO and ZnO:Al bars prepared by photolithography and self-aligned pattern transfer. The roughness of the interfaces is defined by the edge roughness of the structures on the photomask, which had been ink-jet printed in this case.

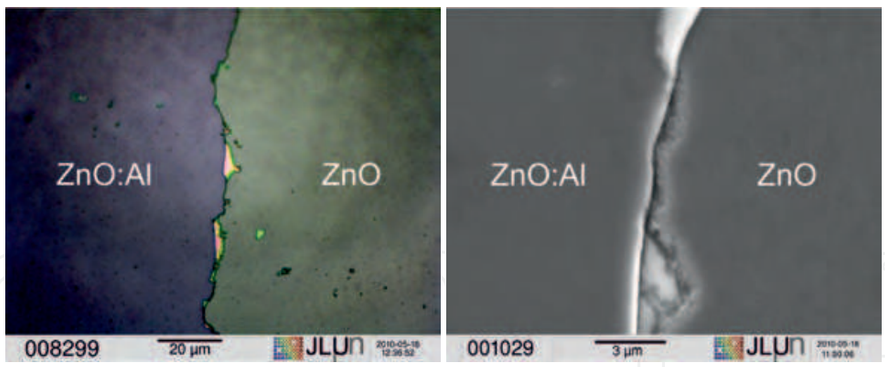

(a) Optical micrograph. (b) Scanning electron micrograph.

Fig. 2. Images of an interface between two conductors with a point-wise contact.

series of four such samples with different numbers of interfaces (2, 4, 8, 16) was prepared. Measurements of the Seebeck coefficient as well as of the electrical conductivity showed that the resistivity decreased with an increasing number of interfaces. In accordance with these results, the absolute values of the Seebeck coefficients decreased with increasing electrical conductivity. Details of the underlying physical effects have been published elsewhere (Homm et al., 2011).

Obviously, there are two length scales at which the properties of the interfaces between the two conductors are determined. On the one hand, there is the roughness of the interface that is determined by the roughness of the edges of the printed structures on the photomask. In a high quality photomask, this roughness is below the wavelength of light and hence negligible, unless an artificial roughness is created intentionally. This roughness would typically be on the micrometer scale, and it determines the length of the resulting interface and hence the area on which transport between the two conductors can occur. On the other hand, there is the length scale of the grain size of the respective conductors and of the average width of the gap between both conductors as a result of the pattern transfer process. At this length scale, the quality of the interface is determined. It can range from an ideal full-contact interface via an interface with an average density of point-wise contacts per unit interface length to a non-contact interface, in which the gap is wider than the typical grain size. An example of a point-wise contacting interface is shown in fig. 2.

In the following sections, we will first describe the sample fabrication procedure, namely the self-aligned pattern transfer. We will then describe how the properties of the interface depend on variations in the process parameters, and which degrees of freedom one has when using this fabrication method. Finally, possible variations and extensions of the technique will be pointed out. It should be noted that the process has been tailored to conductive oxide thin films, but is in principle transferable to other thin film materials.

2. Self-aligned pattern transfer process

Figure 3 shows a somewhat idealized process flow. It starts with the blanket deposition of material A by virtually any thin film deposition method onto a substrate (a). The sample is then coated with photoresist, which is exposed (b) and developed (c). The photoresist masking

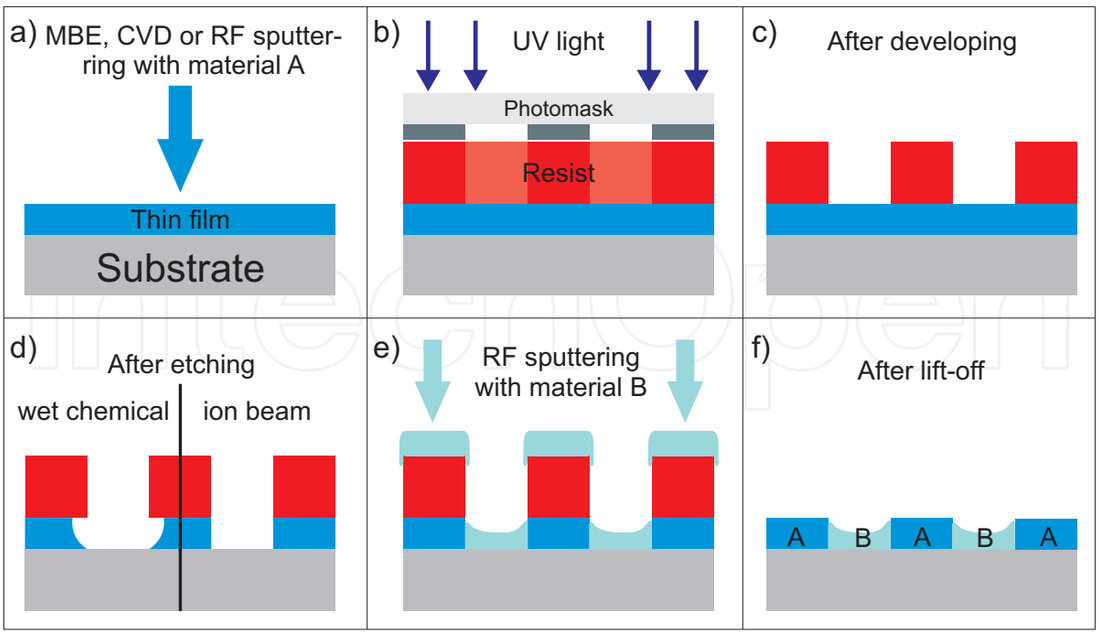

Fig. 3. Lateral patterning of alternating films of two materials by self-aligned pattern transfer.

layer is then used for subtractive patterning of material A, e. g. by wet chemical etching or by ion beam etching (d). The same photoresist masking serves as a lift-off mask in the subsequent additive patterning of material B, consisting of the two steps of thin film deposition (e) and the final lift-off of superfluous material B by dissolving the photoresist masking (f).

In panels (b) and (c) of fig. 3, the assumption has been made that a positive photoresist is used, i. e. a photoresist whose exposed portions are removed during development. As we will see, negative resists can be used as well. In this case, the transparent and opaque structures on the photomask have to be reversed.

The parts of the thin film of material A that are not covered by the patterned photoresist masking are now removed by etching. The etching method may be either wet-chemical etching or any of the wide variety of dry etching methods, such as ion beam etching or reactive ion etching. In the selection of the etching method, two properties have to be considered especially. Firstly, the different etching methods differ in their selectivity, that is the ratio of the etching rate of the thin film (that is to be etched) and of the resist masking (which, ideally, should not be etched at all). Secondly, the different etching methods will deliver differing degrees of anisotropy. In wet-chemical etching, and given that the thin film will be polycrystalline or at best oligocrystalline, etching will be isotropic, i. e., the rate at which the thin film is being removed in horizontal direction will be equal to the rate at which it is etched in vertical direction (Madou, 2002). Ion beam etching, on the other hand, can deliver a certain degree of anisotropy, resulting in steep sidewalls of the etched film and a low degree of underetching (removal of material under the resist masking). The different shapes of the etched thin film are, again somewhat idealized, shown in panel (d) of fig. 3.

The selectivity of the resist masking can be improved by a hardbake procedure, in which the developed sample is heated up to a temperature slightly below the glass point of the resist.

Temperature control must be precise, because at a temperature even slightly too high, the resist masking may lose its shape, resulting in a failure of the remaining processing steps.

While the deposition method for material A can be practically any out of the multitude of methods available for thin films, including the vast class of chemical vapor deposition (CVD) methods or molecular beam epitaxy (MBE), the deposition method for material B has to be compatible with the resist masking still present at this step in the process flow (panel (e) of fig. 3). Namely, the temperature at the sample surface has to remain below the glass point temperature of the photoresist, which usually means a maximum temperature in the range between 120 °C and about 200 °C, dependent on the precise type of resist used. This excludes all CVD and MBE methods and leaves only physical vapor deposition methods (PVD) available. These may be evaporation coating, pulsed laser deposition, or a variety of sputter deposition methods. In the experimental work presented here, material B was always deposited by sputter deposition. The advantages of sputter deposition over evaporation coating are that the resulting films will have a higher degree of crystallinity, and that sputter deposition tends to give a better coverage of sidewalls (conformal coating) than does evaporation coating. This is important since it is usually desirable that the vertical sidewalls of material A make contact to material B. The coverage of the sidewalls may, however, not be too high, since that would mean covering the sidewalls of the resist masking as well, and that would prevent the solvent in the lift-off step (panel (f) of fig. 3) from reaching and hence from dissolving the photoresist. The solvent has to be chosen for good selectivity to the thin film materials and can be either a general purpose solvent such as acetone, or, especially in the case of hardbaked photoresist, a special organic formulation known as “remover”.

3. Freedom of pattern choice and limitations

As mentioned above, the interface shape on a length scale larger than the wavelength of light may be chosen rather arbitrarily. This is demonstrated by the five different interface shapes which were realized and which are shown schematically in fig. 4. The bottom images show optical micrographs of the interface structures transferred into photoresist after the development step. It can be seen that defining these interface shapes on the length scale of a few micrometers is easy with photolithography. Many of the results discussed in the following are based on samples where pattern (d), a wavy interface shape, was used. The alternating bars of the two conductors were designed to cover an area of $5 \times 5\,\mathrm{mm}^2$ between two contact bars each 1 mm wide and extending over the 5 mm perpendicular to the direction of electrical transport. Two orientations of the interfaces to the direction of current flow were implemented, as shown in fig. 5.

The pitch of the conducting bars, or, in other words, their packing density is limited (among others) by the thickness of the thin film of material A. Since, as mentioned above, wet-chemical etching is in many cases nearly perfectly isotropic, the resulting distance between two conductor bar edges at the end of the process flow has to be more than twice the thickness of the thin film. If the structures were too close together, they would either not be separated in the depth of the film (here the surface of the substrate), or they would be damaged near the top film surface once etching has been performed long enough to separate the conducting parts. It should be kept in mind that in order to ensure process safety, given a slight uncertainty in

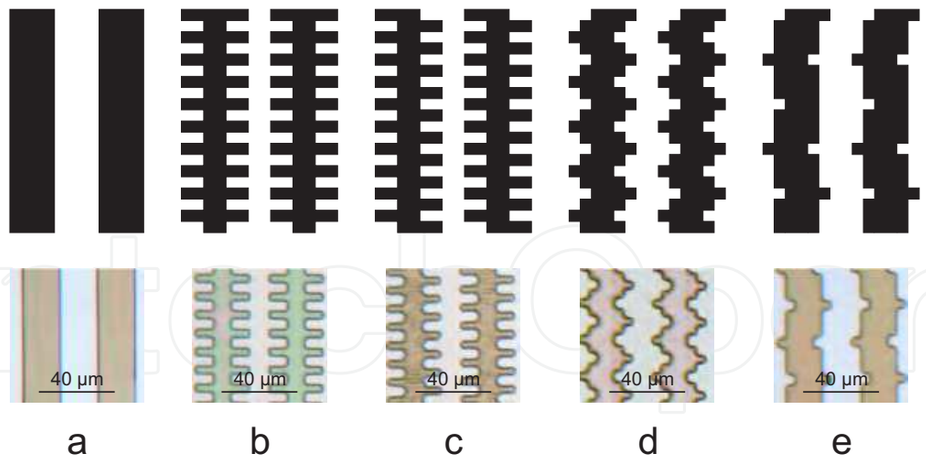

Fig. 4. Schematic drawing of the five different interface shapes designed for structuring of lateral interfaces: (a) straight interfaces, (b) teeth in-phase, (c) teeth in counter-phase, (d) wavy and (e) toothed interfaces with constant distance. The length of a tooth is typically on the order of 5 µm, the pitch (center-to-center-distance of the conducting bars of the same material) on the order of 40 µm. The bottom images are optical micrographs of the pattern transferred into the photoresist after the development step (step c) of fig. 3).

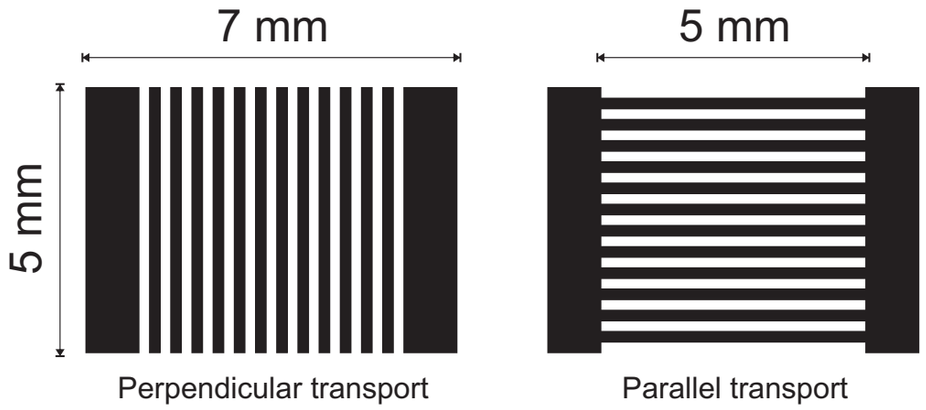

Fig. 5. Schematic drawing of the positioning and orientation of alternating conductor bar structures between the electrical contact bars (to the left and right, respectively).

actual etching rates, etching always has to be carried out for slightly more than the minimum time required theoretically (so-called "overetching").

The etching rate will, among others, depend on the crystallinity of the material being etched. This means that the etching rate of material A will depend on whether it has been deposited with a method like MBE, which gives a high degree of crystallinity and usually lower etch rates, or sputter deposition, which leads to polycrystalline material with a higher etch rate, since etching along the grain boundaries is faster than the etching of the individual grains. As a second-oder effect, the morphology of the etched edge will depend on the deposition method as well. In the case of polycrystalline samples with samples growing predominantly in vertical direction, the conductor edge will be lined with vertical isolated columns, whereas the etched edge of an oligocrystalline film will tend to be rather smooth. Figure 6 depicts

AFM images of etched edges of three ZnO thin-films. The images a) and c) show sputtered ZnO films etched by wet-chemical and ion-beam etching, respectively. Image b) shows an AFM image of a MBE grown ZnO film after wet-chemical etching: The different edge morphologies can be clearly distinguished. The combination of wet-chemical etching and granular sputtered material yields a nanostructured interface region with columns of original material protruding from the closed interface. In contrast, ion-beam etching of sputtered material yields comparatively sharp interfaces with rather steep edges. Wet-chemical etching of epitaxial MBE-grown ZnO shows a closed surface of the edges, but with a smoother slope than for ion-beam etching.

For material B, an upper limit of the film thickness is given by a certain fraction of the thickness of material A. If this fraction exceeds a value around $\frac{3}{4}$, the conformal coating of the resist sidewalls will prevent a succesful lift-off of material B. While the upper limit of the film thickness is governed by the pattern transfer process as described above, the lower limit of the film thickness is given by the requirement that the film be continuous. The limit at which a film becomes continuous varies with the deposition method, and in general, higher deposition temperatures require a larger film thickness to pass the threshold to continuity. Evaporation coating can result in continuous films for thicknesses as low as 10 nm (Völklein & Zetterer, 2006), while for sputter deposition of conducting oxides, the limit is on the order of 50 nm. In addition, a certain minimal film thickness is desirable since the conductivity, which, in first order, is inversely proportional to the film thickness, should not be too low for transport properties to be reliably measurable.

4. Control over the interface properties

In this section we will discuss different combinations of process parameters, namely of the resist and the etching method used, will present the resulting interface morphologies and will correlate the properties to the fabrication process in order to demonstrate the range over which the interface properties can be controlled and tuned.

4.1 Examples of different interface morphologies obtained by a single photolithography step followed by self-aligned pattern transfer

Very often, ***interfaces with point-wise contacts*** are obtained. Two examples are shown in fig. 7 and 8 which were obtained after processing using different photoresists and wet-chemical etching. In the first case the material A consisted of a layer of ZnO with a thickness of 200 nm, grown by molecular beam epitaxy on top of a 300 µm thick sapphire substrate. Photolithography was first performed with a 1.5 µm thick layer of positive photoresist (ma-P 1215 from micro resist technology, Berlin). Exposure was done with a UV broadband source in a Suss MA 56 mask aligner at doses of 67.2 mJ cm^{-2} at 365 nm wavelength and 122.4 mJ cm^{-2} at 405 nm wavelength. The resist was developed in ma-D 331 developer (also from micro resist technology, Berlin) for 15 s and hardbaked for 90 minutes in a convection oven. The zinc oxide was wet-chemically etched in a mixture of 84 % orthophosphoric acid (H_3PO_4), 100 % acetic acid ($C_2H_4O_2$), and water (H_2O) in a ratio of 1:1:100 parts by volume (Elm et al., 2008). Etch end detection could be performed by monitoring the electrical resistance in situ, since ZnO is intrinsically electrically conducting. As material B, a 150 nm thick layer of Ga-doped ZnO was deposited by radio frequency (RF) sputter coating. This thickness is very close to the

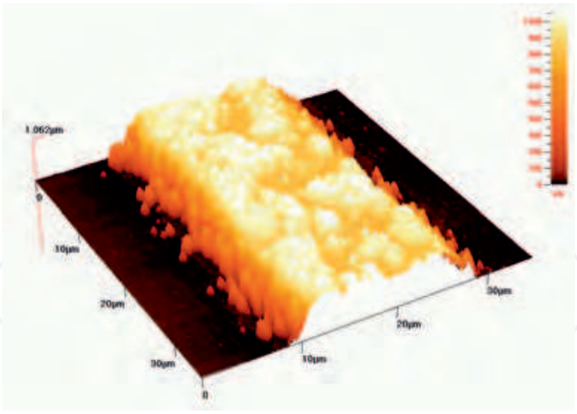

(a) Atomic force micrograph.

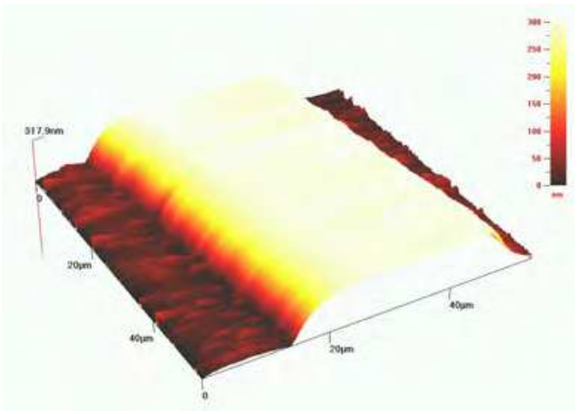

(b) Atomic force micrograph.

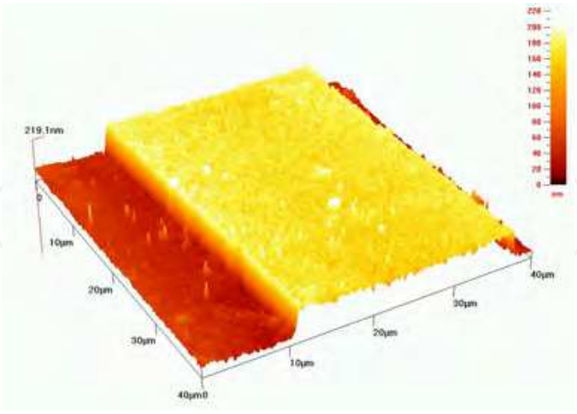

(c) Atomic force micrograph.

Fig. 6. Atomic force microscopy (AFM) images of etched edges of three ZnO thin-films. The images (a) and (b) show a sputtered (a) and an MBE grown (b) film after pattern transfer with wet-chemical etching. Image (c) shows an AFM image of a sputtered ZnO film after pattern transfer by ion-beam etching: The different edge morphologies can be clearly distinguished.

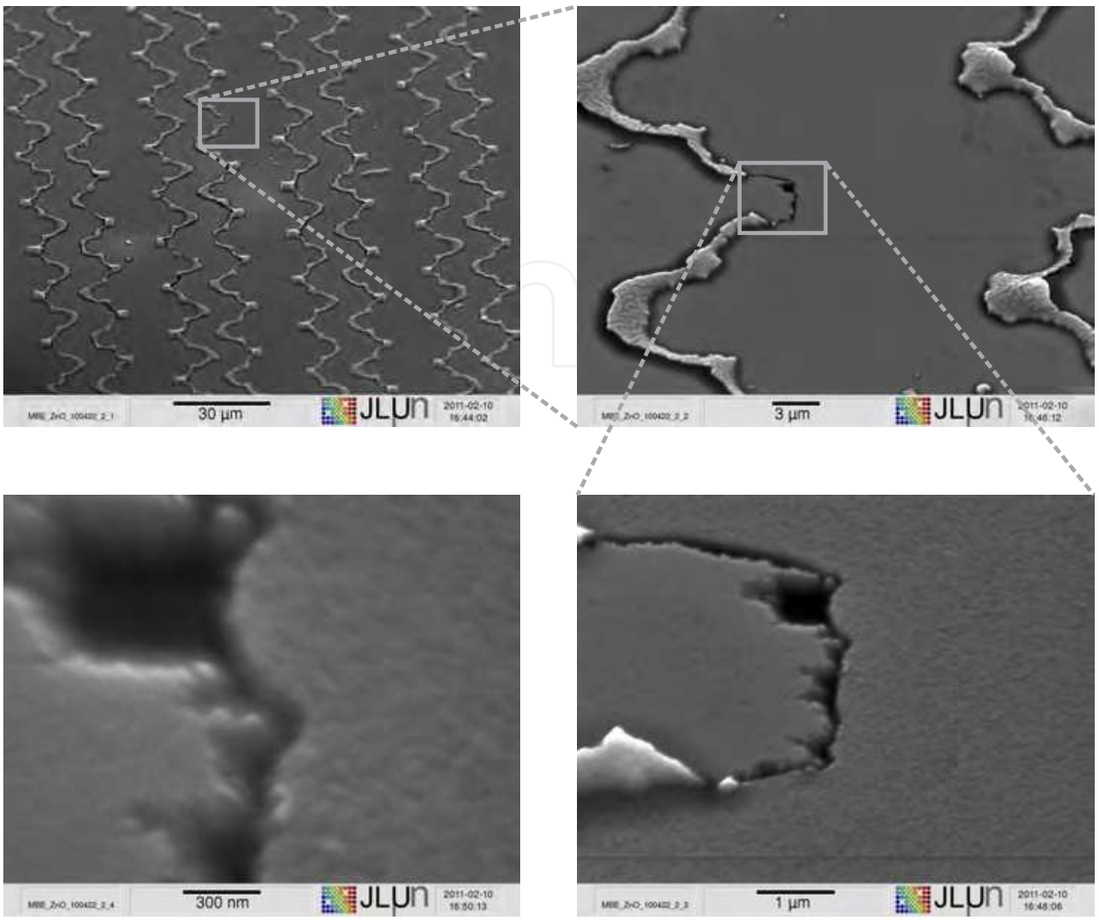

Fig. 7. Scanning electron micrographs (zoom-in series) of a sample with MBE-grown ZnO (material A) and Ga-doped ZnO (material B), processed using positive photoresist and wet-chemical etching. The wavy structures extending over the sample surface are remnants of the sputter coated ZnO layer that had been deposited on the resist sidewalls and hence were not removed in the lift-off step.

limit imposed by the requirement that lift-off still has to be possible. For a succesful lift-off, the solvent bath had to be heated to 50 °C, and ultrasonic excitation had to be applied to the bath.

Figure 7 shows a series of scanning electron micrographs of a sample processed in the way described. At high magnification, the point-wise nature of the contact along the interface is clearly visible. The remnants of the Ga-doped ZnO due to incomplete lift-off (so-called "garden fences", resulting from material deposited on the resist sidewalls) had no influence on the electrical transport properties.

A point-wise contact along the interface similar to that in fig. 7 can also be achieved using negative instead of positive photoresist. The substrate in this experiment was glass, and material A was a thin layer of sputter deposited ZnO. The negative resist ma-N 1420 (again from micro resist technology, Berlin) was spincoated to a thickness of approximately 2 µm and exposed using the same UV broadband source mentioned above, with doses of 560 mJ cm^{-2} at

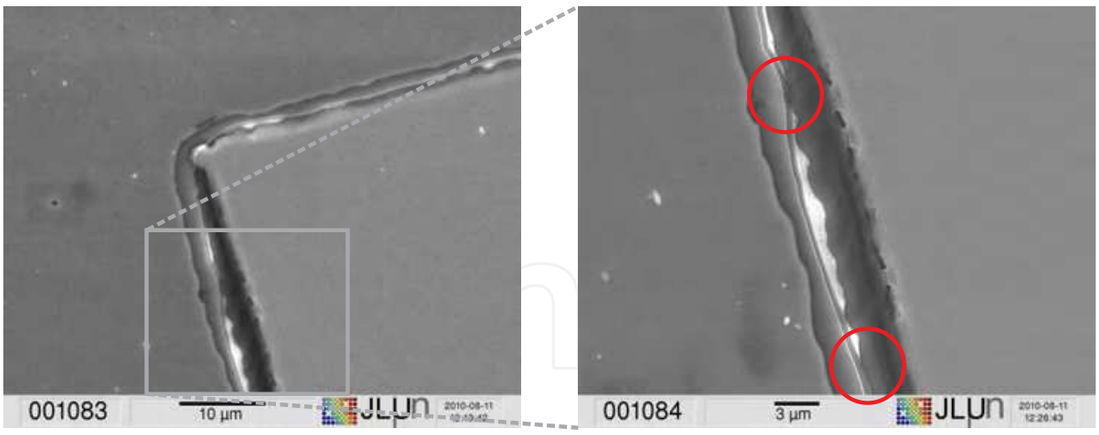

Fig. 8. Scanning electron micrographs (zoom-in) of a sample with sputter deposited ZnO (material A) and sputter deposited Cu_2O (material B), processed using negative photoresist and wet-chemical etching. The point-wise contacts (circled in the right image) had a density of approximately one per 10 µm of interface length.

365 nm wavelength and 1002 mJ cm^{-2} at 405 nm wavelength. The most important parameter is the development time, since this time determines the width of the undercut profile in the developed resist. A development time of 65 s in the developer ma-D 533S (from the same supplier) resulted in an undercut of approximately 0.6 µm (mic, 2011). Again, hardbake has to be subject to tight temperature control in order to preserve the undercut profile. The ZnO was wet-chemically etched as in the experiments with positive photoresist detailed above. Copper-I-oxide (Cu_2O) was sputter coated on the surface. The hardbaked negative resist could not be removed with acetone, so the lift-off was carried out using the specially formulated remover mR-rem 660 (from the same supplier) under ultrasonic excitation. The scanning electron microscopic characterization of the resulting interface, see fig. 8, shows the point-wise nature of the contact, with a contact density of about one per 10 µm of interface length.

Using extreme undercut profiles allows one to separate materials A and B by a gap. Such ***interfaces with a gap*** can be obtained using the same preparation of material A as described in fig. 8, but extending the development time to 120 s. This created a rather extreme undercut of approximately 2.1 µm (mic, 2011). Exposure doses in this case were 504 mJ cm^{-2} (365 nm) and 918 mJ cm^{-2} (405 nm). Material B again was a 150 nm thick layer of Ga-doped ZnO deposited by RF sputter coating. Lift-off was easily achieved with such a large undercut, and fig. 9 shows the result of the complete process in a series of scanning electron micrographs. The isotropic character of the wet-chemical etching process in combination with the undercut profile of the resist sidewalls prevents the creation of interfaces with continuous contact.

Continuous almost ideal interfaces can be obtained by using ion beam etching (IBE) instead of wet-chemical etching as the dry etching avoids an undercut. In IBE, chemically inert ions (Ar^+ in our case) are accelerated by a voltage of several hundred volts (in our case 700 V, in a Kaufman source, at a current density of 190 µA cm^{-2}) and directed onto the sample, resulting in a material removal caused by physical effects ("bombardment") with a certain degree of anisotropy. The etching rate of ZnO under these conditions was approximately 30 nm min^{-1}.

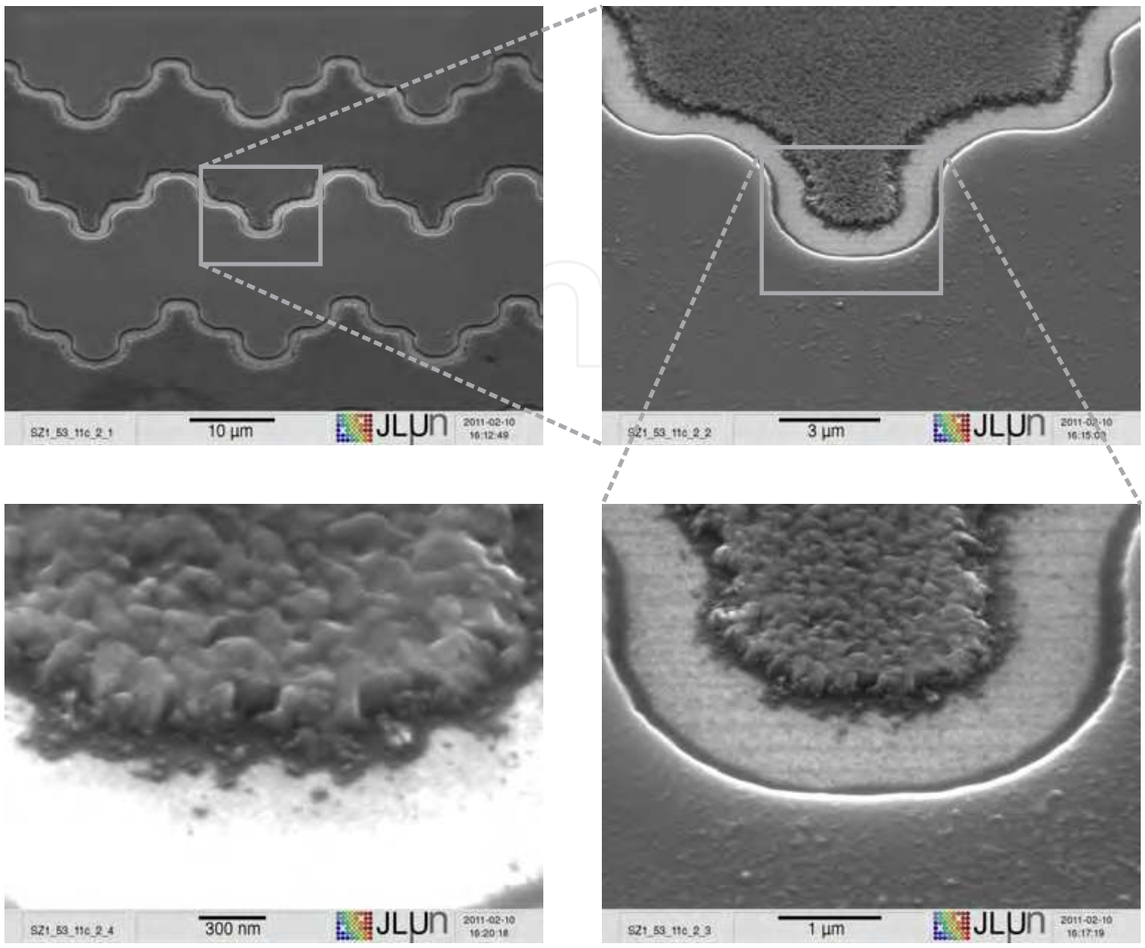

Fig. 9. Scanning electron micrographs (zoom-in series) of a sample with MBE-grown ZnO (material A) and Ga-doped ZnO (material B), processed using negative photoresist and wet-chemical etching. The undercut of the negative resist was tuned to around 2 µm by extending the development time to 120 s, resulting in a well-defined gap along the entire length of the interface.

Alternating etching cycles of no more than 3 minutes and cooling cycles had to be employed to avoid excessive heating of the sample by the ion beam.

The result of a process flow with CVD-grown ZnO (material A), positive photoresist, ion beam etching, and sputter deposited ZnO (material B) is shown in fig. 10. Positive photoresist was used here since in general it provides less undercut than negative resist, which obviously is advantageous for a continuous interface. Lift-off could be achieved with heated acetone under strong ultrasonic excitation. As can be seen in fig. 10, the two materials are in contact along the entire interface, i. e., the combination of photoresist processing and thin film etching method approaches the perfect interface.

Figure 11 summarizes variations of the interface morphology at the submicrometer scale possible with self-aligned pattern transfer based on a single photolithography step.

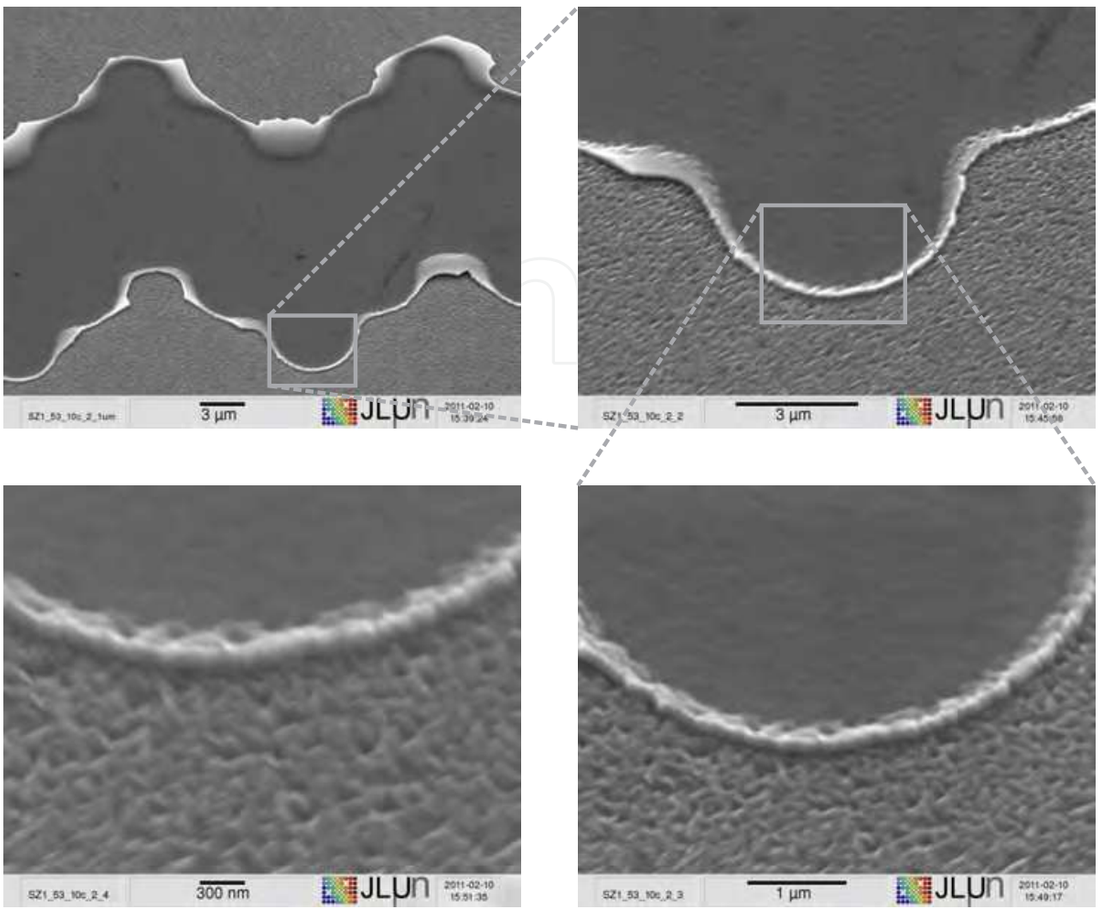

Fig. 10. Scanning electron micrographs (zoom-in series) of a sample with CVD-grown ZnO (material A) and Ga-doped ZnO (material B), processed using positive photoresist and ion beam etching. Some remnants of material B are visible, indicating imperfect lift-off. The two materials are in electrical contact along the entire length of the interface.

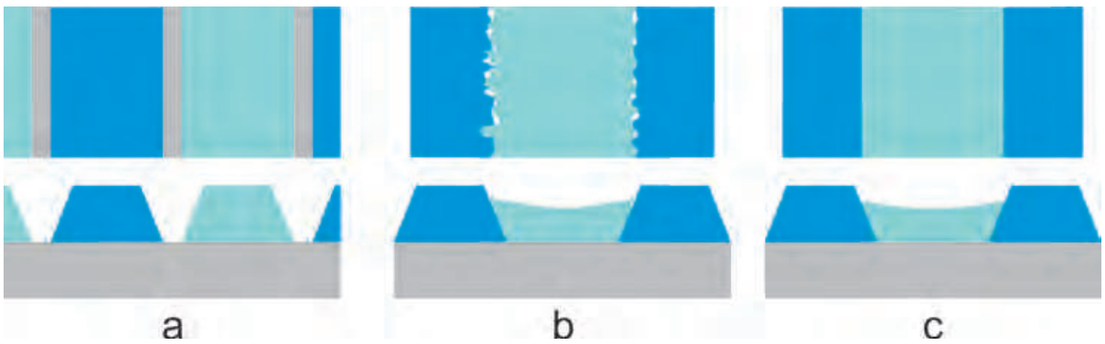

Fig. 11. Interface morphologies realized by a single photolithography step and self-aligned pattern transfer, by variation of the photoresist (undercut profile) and the etching process (anisotropy). From left to right: (a) insulating gap along the length of the interface, (b) point-wise contacts along the length of the interface, and (c) continuous electrical contact over the entire length of the interface.

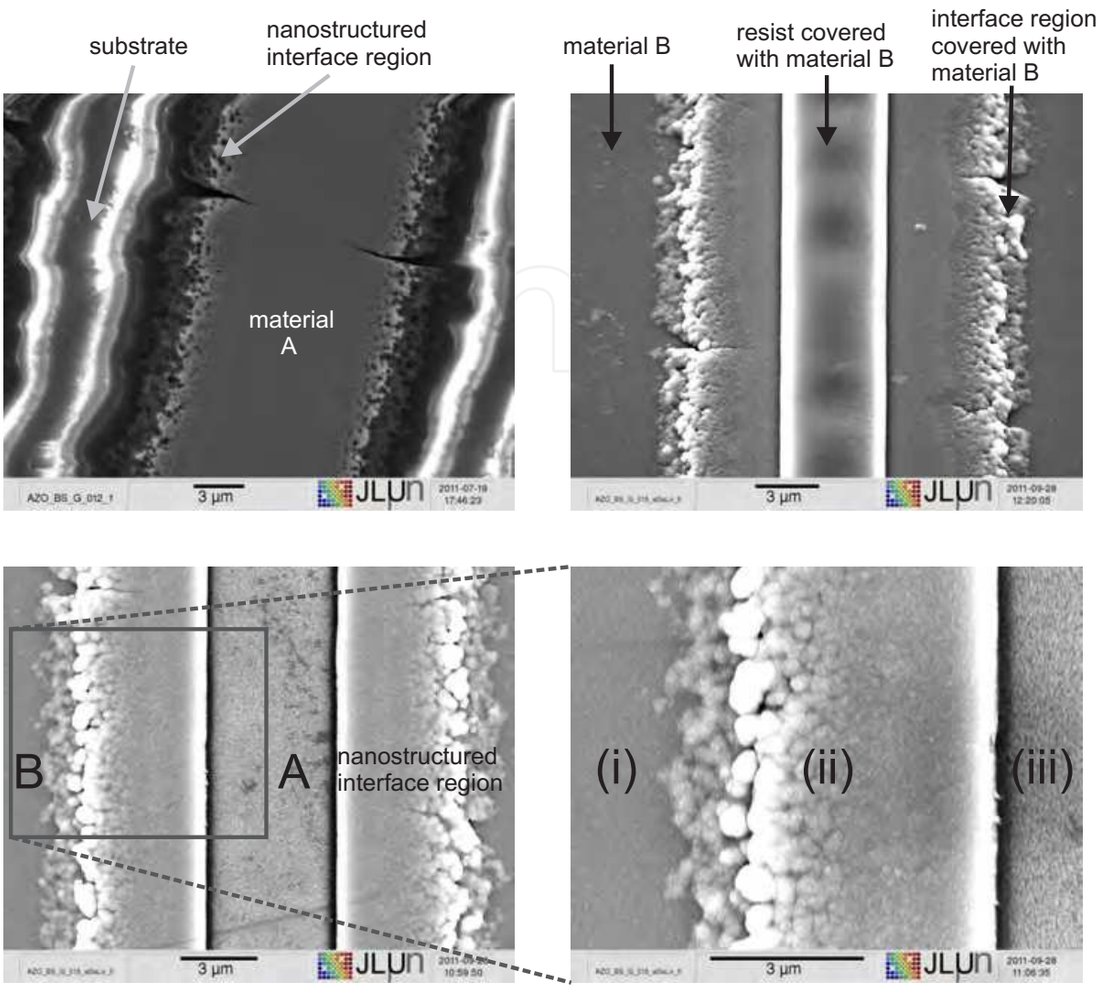

Fig. 12. Scanning electron micrographs of a wet chemically etched layer of ZnO:Al. The four images show samples after different steps of the processing: After wet-chemical etching (upper left), after second lithography and sputter deposition (upper right), after liftoff (lower left), and a magnification of the resulting interface (lower right). The roughness of the edge is predominantly caused by the crystallinity of the material and is on the order of a few tens to about one hundred nanometers.

4.2 Examples of controlled structuring of interfaces on the sub-micrometer scale

In combination with the self-aligned patterning process it is even possible to achieve controlled structure definition of interface regions on the sub-micrometer scale. Here, the possibilities are manifold and we will briefly discuss two examples.

The first example makes use of the properties of wet etching in sputter deposited oxide layers. The grain structure of the oxide thin films is columnar with characteristic diameters of grain columns in the range of 50 to 100 nm. Wet-chemical etching proceeds faster along the grain boundaries than through the nanocrystalline grains, resulting in an irregular array of freestanding nanocrystallites, often columnar in shape, along the edge of the etched thin film, as shown in the SEM image of fig. 12 (top left) and the AFM image in fig. 6 (a). The

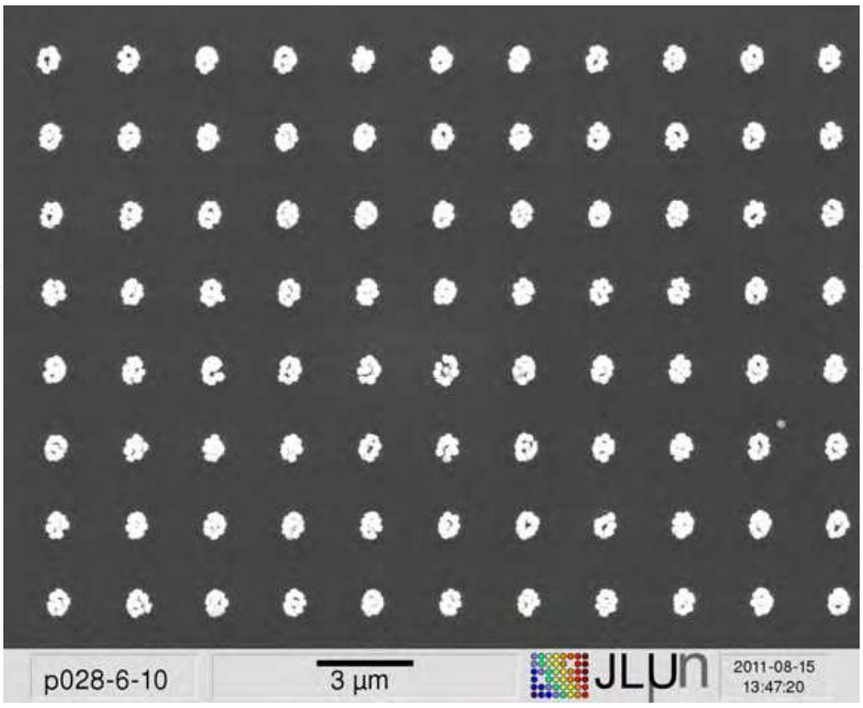

Fig. 13. Gold nanoparticles arranged in circular indentations (arranged on a square grid with 3 µm pitch) in a thin film by the meniscus force method.

width of this region is determined by the characteristic radius of the columnar grains and the ratio of the etch rates along the grain boundaries and through the bulk of the grains. The region can be created in a single photolithography step. Let us assume that the interfaces of a sputter deposited thin film of material A are nanostructured this way, then using the structured film as a starting point of a second lithography step followed by the self-aligned deposition of material B, allows one to embed the nanostructures of material A in the interface region between A and B, yielding a defined interface region. The SEM images of fig. 12 depict different stages of the processing. The magnification of the interface shows three distinct regions: Region (i) is material B coming from the second sputter deposition. Region (ii) is the nanostructured interface, where both materials are on top of each other. In region (iii) material A can be seen. This is the region which was protected by the resist (compare upper right image of fig. 12) and is now uncovered after the lift-off.

The second example may use structures with a well defined gap between A and B (as obtained in fig. 9) as the starting point. Employing a second lithography step to cover the remnants of materials A and B enables one to fill the gap between the two materials (or any other indentation in the photoresist) with nanoparticles. One possibility of achieving the filling in a self-organized way is employing the meniscus force method (Cui et al., 2004; Yin et al., 2001), where during the evaporation of a drop of suspension of nanoparticles, the latter are pushed into the indentations in the sample surface due to the surface tension of the drop. Exemplarily, fig. 13 shows gold nanoparticles self-organized on a substrate with circular indentations. Again, after the gap is filled with nanoparticles a self-aligned deposition of a material C may be carried out to obtain a closed surface.

Fig. 14. Some variations of the interface morphology at the sub-micrometer scale that have been (left) or at the micrometer scale that could be (right) realized with self-aligned pattern transfer. Left: nanocolumnar structures of material A between the areas of bulk materials A and B, respectively. Right: gap between strips of material A filled with nanoparticles before the deposition of material B.

These two examples summarized schematically in fig. 14 demonstrate the potential of integrating the self-aligned pattern transfer method into extended and more complex process schemes.

5. Conclusions and outlook

We have shown how a variety of morphologies of the interface between two conducting oxides can be created by a single photolithography process and subsequent self-aligned pattern transfer. The choice of the process parameters allows one to adjust the morphology of the interfaces ranging from almost ideal interfaces via interfaces with point-wise contacts to interfaces with a gap of controlled width, even below the resolution limit of the photolithographic process step. This is one of the characteristic features of self-aligned pattern transfer.

Incorporating the self-aligned pattern transfer into more complex processing schemes allows one to even achieve controlled interface structuring on the nanometer scale. We have demonstrated that the method of self-aligned pattern transfer offers versatile ways of lateral structuring of thin-film materials.

6. References

Alvarez-Quintana, J., Martínez, E., Pérez-Tijerina, E., Pérez-García, S. A. & Rodríguez-Viejo, J. (2010). Temperature dependent thermal conductivity of polycrystalline ZnO films, *Journal of Applied Physics* 107(6): 063713.
URL: *http://dx.doi.org/doi/10.1063/1.3330755*

Bachmann, M., Czerner, M., Edalati-Boostan, S. & Heiliger, C. (2011). Ab initio calculations of phonon transport in ZnO and ZnS.
URL: *http://arxiv.org/abs/1111.2540*

Bies, W. E., Radtke, R. J. & Ehrenreich, H. (2000). Phonon dispersion effects and the thermal conductivity reduction in GaAs/AlAs superlattices, *Journal of Applied Physics*

88(3): 1498–1503.
URL: *http://dx.doi.org/doi/10.1063/1.373845*

Capinski, W. S., Maris, H. J., Ruf, T., Cardona, M., Ploog, K. & Katzer, D. S. (1999). Thermal-conductivity measurements of GaAs/AlAs superlattices using a picosecond optical pump-and-probe technique, *Phys. Rev. B* 59(12): 8105–8113.
URL: *http://link.aps.org/doi/10.1103/PhysRevB.59.8105*

Chen, G. (1998). Thermal conductivity and ballistic-phonon transport in the cross-plane direction of superlattices, *Phys. Rev. B* 57: 14958–14973.
URL: *http://link.aps.org/doi/10.1103/PhysRevB.57.14958*

Cui, Y., Björk, M. T., Liddle, J. A., Sönnichsen, C., Boussert, B. & Alivisatos, A. P. (2004). Integration of colloidal nanocrystals into lithographically patterned devices, *Nano Letters* 4(6): 1093–1098.
URL: *http://dx.doi.org/10.1021/nl049488i*

Daly, B. C., Maris, H. J., Tanaka, Y. & Tamura, S. (2003). Molecular dynamics calculation of the in-plane thermal conductivity of GaAs/AlAs superlattices, *Phys. Rev. B* 67: 033308.
URL: *http://link.aps.org/doi/10.1103/PhysRevB.67.033308*

Dresselhaus, M., Chen, G., Tang, M., Yang, R., Lee, H., Wang, D., Ren, Z., Fleurial, J.-P. & Gogna, P. (2007). New directions for low-dimensional thermoelectric materials, *Advanced Materials* 19(8): 1043–1053.
URL: *http://dx.doi.org/10.1002/adma.200600527*

Elm, M. T., Henning, T., Klar, P. J. & Szyszka, B. (2008). Effects of artificially structured micrometer holes on the transport behavior of Al-doped ZnO layers, *Applied Physics Letters* 93(23): 232101.
URL: *http://dx.doi.org/doi/10.1063/1.3040312*

Fasol, G., Tanaka, M., Sakaki, H. & Horikoshi, Y. (1988). Interface roughness and the dispersion of confined LO phonons in GaAs/AlAs quantum wells, *Phys. Rev. B* 38: 6056–6065.
URL: *http://link.aps.org/doi/10.1103/PhysRevB.38.6056*

Franz, R. & Wiedemann, G. (1853). Ueber die Wärme-Leitungsfähigkeit der Metalle, *Annalen der Physik* 165(8): 497–531.
URL: *http://dx.doi.org/10.1002/andp.18531650802*

Hicks, L. D. & Dresselhaus, M. S. (1993a). Effect of quantum-well structures on the thermoelectric figure of merit, *Phys. Rev. B* 47(19): 12727–12731.
URL: *http://link.aps.org/doi/10.1103/PhysRevB.47.12727*

Hicks, L. D. & Dresselhaus, M. S. (1993b). Thermoelectric figure of merit of a one-dimensional conductor, *Phys. Rev. B* 47(24): 16631–16634.
URL: *http://link.aps.org/doi/10.1103/PhysRevB.47.16631*

Hillmer, H., Forchel, A., Sauer, R. & Tu, C. W. (1990). Interface-roughness-controlled exciton mobilities in GaAs/$Al_{0.37}Ga_{0.63}As$ quantum wells, *Phys. Rev. B* 42: 3220–3223.
URL: *http://link.aps.org/doi/10.1103/PhysRevB.42.3220*

Homm, G., Petznick, S., Gather, F., Henning, T., Heiliger, C., Meyer, B. K. & Klar, P. J. (2011). Effect of Interface Regions on the Thermoelectric Properties of Alternating ZnO/ZnO:Al Stripe Structures, *Journal of Electronic Materials* 40: 801–806.
URL: *http://dx.doi.org/10.1007/s11664-011-1574-4*

Huang, Z. X., Tang, Z. A., Yu, J. & Bai, S. (2011). Thermal conductivity of nanoscale polycrystalline ZnO thin films, *Physica B: Condensed Matter* 406(4): 818 – 823.
URL: *http://www.sciencedirect.com/science/article/pii/S0921452610011671*

Igamberdiev, K. T., Yuldashev, S. U., Kurbanov, S. S., Kang, T. W., Khabibullaev, P. K., Rakhimova, S. M., Pelenovich, V. O. & Shashkov, A. G. (2010). Thermal properties of semiconductor zinc oxide nanostructures, *Journal of Engineering Physics and Thermophysics* 83(4): 863 – 868.
URL: *http://dx.doi.org/10.1007/s10891-010-0407-2*

Lorenz, L. (1872). Bestimmung der Wärmegrade in absolutem Maaße, *Annalen der Physik* 223(11): 429–452.
URL: *http://dx.doi.org/10.1002/andp.18722231107*

Madou, M. J. (2002). *Fundamentals of Microfabrication - The Science of Miniaturization*, CRCPress.

mic (2011). *ma-N 400 and ma-N 1400 - Negative Tone Photoresists*.
URL: *http://www.microresist.de/products/negative_photoresists/pdf/po_pi_1400_400_man_08041003_en_ls.pdf*

Müller, W., Bertram, D., Grahn, H. T., von Klitzing, K. & Ploog, K. (1994). Competition between thermally induced resonant tunneling and phonon-assisted tunneling in semiconductor superlattices, *Phys. Rev. B* 50: 10998–11001.
URL: *http://link.aps.org/doi/10.1103/PhysRevB.50.10998*

Schwartz, A. (1998). The potential engineering of grain boundaries through thermomechanical processing, *JOM Journal of the Minerals, Metals and Materials Society* 50: 50–55.
URL: *http://dx.doi.org/10.1007/s11837-998-0250-5*

Sootsman, J. R., Chung, D. Y. & Kanatzidis, M. G. (2009). Alte und neue Konzepte für thermoelektrische Materialien, *Angewandte Chemie* 121: 8768–8792.
URL: *http://dx.doi.org/10.1002/ange.200900598*

Venkatasubramanian, R. (2000). Lattice thermal conductivity reduction and phonon localization like behavior in superlattice structures, *Phys. Rev. B* 61(4): 3091–3097.
URL: *http://link.aps.org/doi/10.1103/PhysRevB.61.3091*

Venkatasubramanian, R., Siivola, E., Colpitts, T. & O'Quinn, B. (2001). Thin-film thermoelectric devices with high room-temperature figures of merit, *Nature* 413(6856): 597–602.
URL: *http://dx.doi.org/10.1038/35098012*

Völklein, F. & Zetterer, T. (2006). *Praxiswissen Mikrosystemtechnik*, Vieweg Praxiswissen.

Watanabe, T. (1985). Structural effects on grain boundary segregation, hardening and fracture, *Journal de Physique Colloques* 46(C4): C4–555–C4–566.
URL: *http://hal.archives-ouvertes.fr/jpa-00224714/en/*

Watanabe, T. (1993). Grain boundary design and control for high temperature materials, *Materials Science and Engineering: A* 166(1-2): 11–28.
URL: *http://www.sciencedirect.com/science/article/pii/092150939390306Y*

Watanabe, T. & Tsurekawa, S. (1999). The control of brittleness and development of desirable mechanical properties in polycrystalline systems by grain boundary engineering, *Acta Materialia* 47(15-16): 4171–4185.
URL: *http://www.sciencedirect.com/science/article/pii/S135964549900275X*

Yang, B. & Chen, G. (2003). Partially coherent phonon heat conduction in superlattices, *Phys. Rev. B* 67: 195311.
URL: *http://link.aps.org/doi/10.1103/PhysRevB.67.195311*

Yao, T. (1987). Thermal properties of AlAs/GaAs superlattices, *Applied Physics Letters* 51(22): 1798–1800.
URL: *http://dx.doi.org/doi/10.1063/1.98526*

Yin, Y., Lu, Y., Gates, B. & Xia, Y. (2001). Template-assisted self-assembly: A practical route to complex aggregates of monodispersed colloids with well-defined sizes, shapes, and structures, *Journal of the American Chemical Society* 123(36): 8718–8729.
URL: *http://dx.doi.org/10.1021/ja011048v*

Materials Science and Technology
Edited by Prof. Sabar Hutagalung

ISBN 978-953-51-0193-2
Hard cover, 324 pages
Publisher InTech
Published online 07, March, 2012
Published in print edition March, 2012

Materials are important to mankind because of the benefits that can be derived from the manipulation of their properties, for example electrical conductivity, dielectric constant, magnetization, optical transmittance, strength and toughness. Materials science is a broad field and can be considered to be an interdisciplinary area. Included within it are the studies of the structure and properties of any material, the creation of new types of materials, and the manipulation of a material's properties to suit the needs of a specific application. The contributors of the chapters in this book have various areas of expertise. therefore this book is interdisciplinary and is written for readers with backgrounds in physical science. The book consists of fourteen chapters that have been divided into four sections. Section one includes five chapters on advanced materials and processing. Section two includes two chapters on bio-materials which deal with the preparation and modification of new types of bio-materials. Section three consists of three chapters on nanomaterials, specifically the study of carbon nanotubes, nano-machining, and nanoparticles. Section four includes four chapters on optical materials.

INTECH
open science | open minds

InTech Europe
University Campus STeP Ri
Slavka Krautzeka 83/A
51000 Rijeka, Croatia
Phone: +385 (51) 770 447
Fax: +385 (51) 686 166
www.intechopen.com

InTech China
Unit 405, Office Block, Hotel Equatorial Shanghai
No.65, Yan An Road (West), Shanghai, 200040, China
中国上海市延安西路65号上海国际贵都大饭店办公楼405单元
Phone: +86-21-62489820
Fax: +86-21-62489821

IntechOpen